2. SEW2871 (5 mg/kg; Cayman Chemical) dissolved in a vehicle (PBS containing 5% acidified DMSO and 3% fatty acid-free BSA) or vehicle (23).
3. JTE013 (3 mg/kg; Tocris Bioscience) dissolved in a vehicle (PBS containing 5% acidified DMSO and 3% fatty acid-free BSA) or vehicle (24).
4. GST-RANKL (2 mg/kg, dissolved in PBS) (28).
5. 29- or 30-G insulin syringes (Becton Dickinson).
6. An indwelling needle: a 30-G needle attached to PE-10 tubing (Becton Dickinson).

2.6. Image Analysis

1. Imaging analysis software: Imaris (Bitplane) or Volocity (PerkinElmer).
2. After Effects (Adobe).

2.7. In Vitro Migration Assay

1. EZ-TAXIScan (Effector Cell Institute, GE HealthCare; see Note 10) containing "41 Glass," a small O-shaped ring, an EZ-TAXIScan chip, a rubber gasket, a holder base, wafer housing, a wafer clamp, a syringe guide, and a large O-shaped ring.
2. Sample loading tip attached to a plastic syringe (Becton Dickinson).
3. Microsyringe (10 μL; MS-E10MIC; Exmire).
4. 25-mm Thermanox plastic coverslip (Nunc; see Note 11).
5. Scissors and tweezers.
6. Serum-free Dulbecco's modified Eagle's medium (DMEM).
7. Serum-free alpha-minimum essential medium (αMEM) and αMEM with 10% fetal calf serum (FCS), containing 1% penicillin and streptomycin.
8. PBS, pH 7.4.
9. 0.02% EDTA in PBS.
10. Raw 264.7 cells (American Type Culture Collection, ATCC).
11. Male or female C57BL/6 mice (6-9 weeks old).
12. Syringe with 26-G needle.
13. Mouse recombinant macrophage colony-stimulating factor (M-CSF; 100 ng/mL; PeproTech).
14. Chemoattractant: S1P (10^{-6}, 10^{-7}, and 10^{-8} M; Enzo Life Sciences), dissolved in a vehicle (DMEM; see Note 12).
15. ImageJ software (National Institutes of Health, NIH), equipped with an add-on program, MT Track J.

3. Methods

3.1. Intravital Two-Photon Imaging

1. Start up the two-photon microscope and turn on the heater in the environmental chamber (see Note 13).
2. All the procedures on mice are performed under anesthesia (see Note 14). Shave the hair and apply hair-removal lotion on top of the mouse's head (see Note 15). Cut the skin minimally with iris scissors for insertion of the O-ring. Fix the O-ring on the parietal bone with adhesive and petrolatum or difloil grease (see Note 16), which prevents leakage of PBS and fills the O-ring.
3. Insert an indwelling needle into the tail vein to treat the mouse with reagents during observation.
4. Intravenously inject 100 μL of 2 mg/mL 70-kDa Texas Red-conjugated dextran in PBS (see Note 17).
5. Immobilize the mouse on the custom-made stereotactic holder as tightly as possible to avoid drift owing to respiration and pulsation (Fig. 1; see Note 18).
6. Focus on the bone marrow cavity at an appropriate depth and look through ocular lenses with the help of a mercury lamp. Change the light source from the mercury lamp to the Ti-Sapphire laser and the optical path to the NDD. Set the zoom ratio, z-positions, the interval time, and the duration time using observation software attached to the microscope (Fig. 2).
7. Inject 100 μL of each reagent per mouse.
8. Analyze images by measuring cellular velocities, migration lengths, and contact times using image processing and analysis software.

3.2. In Vitro Migration Assay

3.2.1. Bone Marrow-Derived M-CSF-Dependent Mononuclear Cells

1. Harvest bone marrow cells from C57BL/6 mice by flushing serum-free αMEM medium using a 26-G syringe.
2. Wash the harvested cells twice with αMEM containing FCS and culture the cells in αMEM containing FCS and 100 ng/mL M-CSF for 3 days.
3. Wash cells once with PBS and treat them with 0.02% EDTA in PBS.
4. Collect suspended cells and culture them in αMEM containing FCS and 100 ng/mL M-CSF for another 3 days.

3.2.2. Setting of EZ-TAXIScan

1. Place "41 Glass" in holder base. Drop DMEM in the center of the glass and place a coverslip over the liquid (see Note 19). Wipe off excess fluid, making sure no air bubbles are trapped between the glasses.

Fig. 2. Osteoclast precursors visualized by intravital two-photon imaging. Murine parietal bone of heterozygous Cx_3CR1-EGFP knock-in mice is visualized. CX_3CR1-EGFP-positive cells appear *green* in the bone marrow cavity. Collagen fibers in bone are detected by second-harmonic generation (*in blue*) and the blood vessels are visualized by 70-kDa dextran-conjugated Texas Red.

2. Place the small "O-shaped ring" on top of the wafer housing. Gently close the inner lever and fix the wafer housing.
3. Fill inside the wafer housing with 4 mL of DMEM.
4. Place the EZ-TAXIScan chip gently into the wafer housing (see Note 20), making sure no air bubbles are trapped. To protect the chip, place the rubber gasket beneath the wafer clamp. Place wafer clamp on wafer housing. Place the large O-shaped ring upside of the wafer housing. Gently close the outer lever (see Note 21).
5. Place the assembled device on top of the preheated EZ-TAXIScan microscope.

3.2.3. Alignment of Cells

1. Remove 1 mL of medium from the upper side of the holder.
2. Add 1 µL of cells (Raw 264.7 cells or bone-marrow derived M-CSF-dependent mononuclear cells) to the second chamber using a microsyringe with a syringe guide.

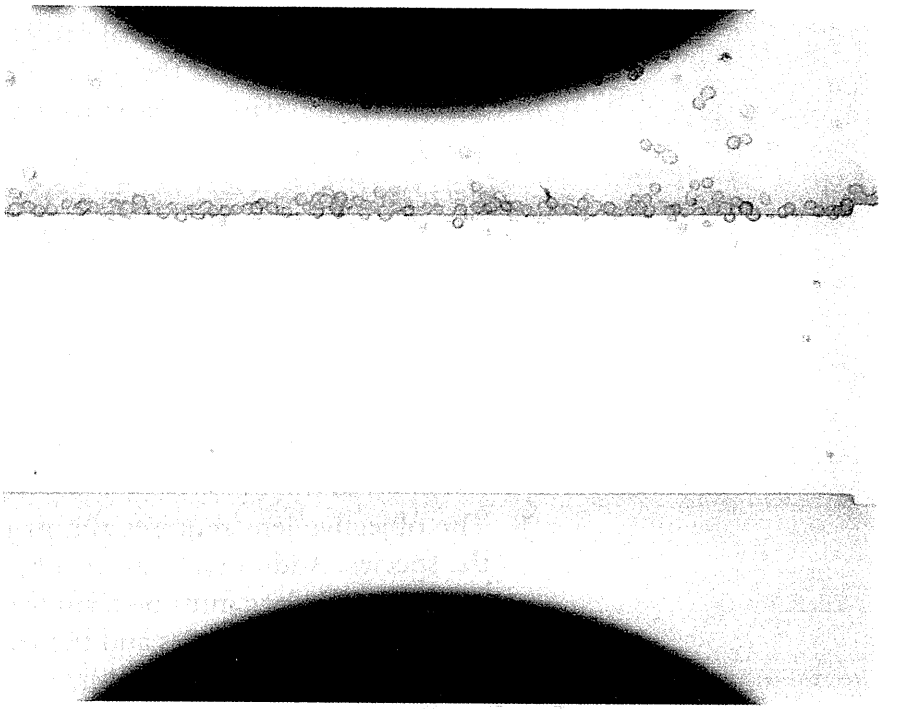

Fig. 3. Alignment of cells on one side of the EZ-TAXIScan chip before analysis. Before analysis of cell migration, cells should be aligned in the chamber on one side.

3. Remove 8–10 μL of medium from the third chamber using a microsyringe.
4. Monitor alignment of the cells on one side (Fig. 3).
5. Return the removed medium inside the holder.

3.2.4. Analysis of Chemotaxis

1. Begin image acquisition using 1-min intervals.
2. Add 1 ml of the chemoattractant (S1P: 10^{-6}, 10^{-7}, and 10^{-8} M) to the third chamber.
3. Sequential image data are processed and migration speeds and tracking distances are calculated using analysis software.

4. Notes

1. The two-photon microscopy setup is also available from other microscope manufacturers (Zeiss, Nikon, and Olympus). Regarding objective lenses, higher NA and longer WD should be desirable. Bone marrow can be observed through an inverted microscope.
2. A femtosecond-pulsed infrared laser is also available from Coherent (Chameleon).
3. The more channels the NDD has, the more colors can be detected.

4. As sufficient space is necessary to place a living mouse between the objective lens and the stage, we replaced the normal stage for the section with a customized one.
5. Because temperature is a critical factor for cell mobility, a decrease in body temperature of the animal must be prevented. Thus, we set up an environmental chamber, which can enclose the animal with the microscope stage and the objective lens.

[AU2]

6. Global S1PR1 deficiency causes embryonic lethally at e12.5 to e14.5 due to defective blood vessel development (29).
7. Although S1PR2-deficient mice suffer from auditory impairment due to vessel defects in the inner ear, they survive and reproduce (25).
8. The objective lens requires almost the same WD as that from the species. Additionally, as the objective lens is water immersible, the substance must be filled with the same refractive index as water between species and the lens. The O-ring works both as a spacer and a PBS reservoir.
9. We used a red dye in this protocol because the target cells express EGFP. If the target cells are red, dextran-conjugated fluorescein isothiocyanate (FITC) can be used. Far-red dyes, such as Qdot-650, can be an alternative if the NDD has a channel that can detect long-wavelength signals. As blood vessels inside the bone marrow cavity have relatively high permeability, dextran with molecular weights over 70 kDa should be used.
10. The EZ-TAXIscan is a visually accessible chemotactic chamber in which one compartment containing ligand (for example, S1P of various concentrations) and another compartment containing cells are connected by a microchannel. A stable concentration gradient of chemoattractant can be reproducibly formed and maintained through the channel without medium flow. Phase-contrast images of migrating cells are acquired at 1-min intervals.
11. 0.2 mm-thick cover slips coated with other reagents (such as collagen and fibronectin) can also be used.
12. Stock solutions of S1P are difficult to make. To accomplish this, S1P should be dissolved in BSA (4 mg/mL)-containing buffers or in other organic solvents with sonication or gentle warming (at 45–60°C).
13. It takes some time for the laser and the temperature to stabilize.
14. All animals must be handled according to institutional and national guidelines and regulations under an approved protocol.
15. Remove hair as much as possible to avoid hair coming into the visual field because it produces strong background autofluorescence.

16. Avoid glue contamination of the visual fields: some glues can produce autofluorescence.
17. With excretion of the dextran into urine, fluorescence fades after several hours. If necessary, additional dosage of the dye should be added.
18. Do not fasten too tightly because the animal can be hurt.
19. The coated side should be set upward.
20. The EZ-TAXIScan chip should be handled gently with tweezers. To protect it from drying, place it in a liquid at all times. After using, the EZ-TAXIScan chip should be sonicated and stored in 20–70% ethanol at room temperature. There are four types of EZ-TAXIScan chips with depths of 4, 5, 6, and 8 μm. The suitable size depends on the cell types. The 8-μm-depth chip should be used for Raw 264.7 cells and 5-μm-depth chip for bone marrow-derived M-CSF-dependent mononuclear cells.
21. Before setting up the assembled device, make sure no air bubbles remain inside the chamber. If air bubbles are present, remove them with the sample-loading tip attached to the plastic syringe.

Acknowledgment

This work was supported by Grants-in-Aid for Encouragement of Young Scientists (A) (22689030), for Scientific Research on Innovative Areas (22113007) and by a Funding Program for World-Leading Innovative R&D on Science and Technology (FIRST Program) from the Ministry of Education, Science, Sports and Culture of Japan, by a Grant-in-Aid for Research on Allergic Disease and Immunology (H21-010) from the Ministry of Health, Labor and Welfare of Japan, and by Grants from the International Human Frontier Science Program (CDA-00059/2009 and RGY-0077/2011).

References

1. Harada S, Rodan GA (2003) Control of osteoblast function and regulation of bone mass. Nature 423:349–355
2. Teitelbaum SL, Ross FP (2003) Genetic regulation of osteoclast development and function. Nat Rev Genet 4:638–649
3. Henriksen K et al (2009) Local communication on and within bone controls bone remodeling. Bone 44:1026–1033
4. Yu X et al (2003) Stromal cell-derived factor-1 (SDF-1) recruits osteoclast precursors by inducing chemotaxis, matrix metalloproteinase-9 (MMP-9) acrivity, and collagen transmigration. J Bone Miner Res 18:1404–1418
5. Wright LM et al (2005) Stromal cell-derived factor-1 binding to its chemokine receptor CXCR4 on precursor cells promotes the chemotactic recruitment, development and survival of human osteoclasts. Bone 36:840–853
6. Koizumi K et al (2009) Role of CX3CL1/fractalkine in osteoclast differentiation and bone resorption. J Immunol 183:7825–7831

7. Kim MS, Day CJ, Morrison NA (2005) MCP-1 is induced by receptor activator of nuclear factor-kB ligand, promotes human osteoclast fusion, and rescues granulocyte macrophage colony-stimulating fctor suppression of osteoclast formation. J Biol Chem 280: 16163–16169
8. Choi SJ et al (2000) Macrophage inflammatory protein 1-α is a potential osteoclast stimulatory factor in multiple myeloma. Blood 96: 671–675
9. Lean JM et al (2002) CCL9/MIP-1 gamma and its receptor CCR1 are the major chemokine ligand/receptor species expressed by osteoclasts. J Cell Biochem 87:386–393
10. Ha J et al (2010) CXC chemokine ligand 2 induced by receptor activator of NF-κB ligand enhances osteoclastogenesis. J Immunol 184: 4717–4724
11. Kwak HB et al (2008) Reciprocal cross-talk between RANKL and interferon-gamma-inducible protein 10 is responsible for bone-erosive experimental arthritis. Arthritis Rheum 58:1332–1342
12. Binder NB et al (2009) Estrogen-dependent and C-C chemokine receptor-2-dependent pathways determine osteoclast behavior in osteoporosis. Nat Med 15:417–424
13. Ishii M et al (2009) Sphingosine-1-phospate mobilizes osteoclast precursors and regulates bone homeostasis. Nature 458:524–528
14. Ishii M et al (2010) Chemorepulsion by blood S1P regulates osteoclast precursor mobilization and bone remodeling in vivo. J Exp Med 207:2793–2798
15. Cahalan MD et al (2002) Two-photon tissue imaging: seeing the immune system in a fresh light. Nat Rev Immunol 2:872–880
16. Germain RN et al (2006) Dynamic imaging of the immune system: progress, pitfalls and promise. Nat Rev Immunol 6:497–507
17. Wang BG, Konig K, Halbhuber KJ (2010) Two-photon microscopy of deep intravital tissues and its merits in clinical research. J Microsc 238:1–20
18. Germain RN et al (2008) Making friends in out-of-the-way places: how cells of the immune system get together and how they conduct their business as revealed by intravital imaging. Immunol Rev 221:163–181
19. Jung S et al (2000) Analysis of fractalkine receptro CX_3CR1 function by targeted deletion and green fluorescent protein reporter gene insertion. Mol Cell Biol 20:4106–4114
20. Burnett SH et al (2004) Conditional macrophage ablation in transgenic mice expressing a Fas-based suicide gene. J Leukoc Biol 75: 612–623
21. Rivera J, Proia RL, Olivera A (2008) The alliance of sphingosine-1-phosphate and its receptors in immunity. Nat Rev Immunol 8:753–763
22. Matloubian M et al (2004) Lymphocyte egress from thymus and peripheral lymphoid organs is dependent on S1P receptor 1. Nature 6972:355–360
23. Wer SH et al (2005) Sphingosine 1-phospate type 1 receptor agonism inhibits transendothelial migration of medullary T cells to lymphatic sinuses. Nat Immunol 12:1228–1235
24. Osaka M et al (2002) Enhancement of sphingosine 1-phosphate-induced migration of vascular endothelial cells and smooth muscle cells by an EDG-5 antagonist. Biochem Biophys Res Commun 299:483–487
25. Allende M et al (2003) G-protein-coupled receptor $S1P_1$ acts within endothelial cells to regulate vascular maturation. Blood 102: 3665–3667
26. Ferron M, Vacher J (2005) Targeted expression of Cre recombinase in macrophages and osteoclasts in transgenic mice. Genesis 41: 138–145
27. Kono M et al (2007) Deafness and stria vascularis defects in $S1P_2$ receptor-null mice. J Biol Chem 282:10690–10696
28. Tomimori Y et al (2009) Evaluation of pharmaceuticals with a novel 50-hour animal model of bone loss. J Bone Miner Res 24: 1194–1205
29. Liu Y et al (2000) Edg-1, the G-protein-coupled receptor for sphingosine-1-phosphate, is essential for vascular maturation. J Clin Invest 106:951–961

Rheumatol Int
DOI 10.1007/s00296-012-2397-1

ORIGINAL ARTICLE

Baseline anti-citrullinated peptide antibody (ACPA) titers and serum interleukin-6 (IL-6) levels possibly predict progression of bone destruction in early stages of rheumatoid arthritis (ERA)

Yukihiko Saeki · Eriko Kudo-Tanaka · Shiro Ohshima · Masato Matsushita · So-ichiro Tsuji · Yu-ichi Maeda · Maiko Yoshimura · Akane Watanabe · Yoshinori Katada · Yoshinori Harada · Kenji Ichikawa · Yasuo Suenaga · Yusuke Ohta · Shigeto Tohma · NHO iR-net Study Group

Received: 25 October 2011 / Accepted: 11 March 2012

Abstract A prospective study was made to seek for a convenient biomarker to predict progression of bone destruction (PBD) in early stages of rheumatoid arthritis (ERA). All participated patients had definite RA and their radiographic stages were mild less than stage II of the Steinbrocker classification, naïve for treatment of any DMARDs or corticosteroids. After the entry, they were treated according to the 2002 ACR management guideline for RA. The candidate biomarkers (RF-IgM, RF-IgG, CARF, ACPA, CRP, ESR, NTx, MMP-3, IL-6 and osteopontin) were measured at the entry. PBD was assessed radiographically by interval changes in the modified Sharp scores (ΔSHS) for 24 months. The associations between ΔSHS and baseline biomarkers were assessed statistically by multivariate regression analyses. Both the baseline ACPA and IL-6 levels correlated with PBD, suggesting that they could predict PBD in ERA.

Keywords Rheumatoid arthritis · Bone/joint destruction · Biomarker · Prediction · Anti-citrullinated peptide antibody (ACPA) · Interleukin-6 (IL-6)

Y. Saeki (✉) · S. Ohshima
Department of Clinical Research, National Hospital Organization (NHO) Osaka Minami Medical Center, 2-1 Kidohigashi-machi, Kawachinagano City, Osaka 586-8521, Japan
e-mail: saekiy@ommc-hp.jp

Y. Saeki · E. Kudo-Tanaka · S. Ohshima · M. Matsushita · S. Tsuji · Y. Maeda · M. Yoshimura · A. Watanabe
Department of Rheumatology, National Hospital Organization (NHO) Osaka Minami Medical Center, Osaka, Japan

Y. Katada · Y. Harada
Department of Allergology, National Hospital Organization (NHO) Osaka Minami Medical Center, Osaka, Japan

K. Ichikawa
Department of Rheumatology, NHO Hokkaido Medical Center, Sapporo, Japan

Y. Suenaga
Department of Rheumatology, NHO Beppu Medical Center, Beppu, Japan

Y. Ohta
Department of Rheumatology, NHO Minami-Okayama Medical Center, Okayama, Japan

S. Tohma
Department of Rheumatology, NHO Sagamihara Hospital, Sagamihara, Japan

Introduction

Rheumatoid arthritis (RA) is a systemic autoimmune disease of unknown origin characterized by chronic destructive polyarthritis which leads to disability and increased mortality. Although its etiology is unknown, the disease is thought to develop through three main processes such as autoimmunity, inflammation and subsequent bone resorption. On the other hand recent cumulative evidence suggests that early diagnosis and therapeutic interventions at the early stages of RA are important [1]. However, clinical course or prognosis of RA is not uniform but various. Therefore, the individual patient needs an optimal therapeutic strategy according to their prognosis. In order for this, the individual clinical course or prognosis should be predicted accurately. Although several candidate predictive biomarkers have been reported, none has been definite [2].

The aim of this prospective study was to seek for a useful biomarker measurable in the blood samples to

Published online: 29 March 2012

predict progression of bone destruction (PBD) in mild radiographic stages of RA under the real clinical circumstances. The representative biomarkers were selected as a candidate according to the main disease processes such as autoimmunity, inflammation and bone resorption.

Materials and methods

Subjects

This study has been approved by the Ethical Committee of NHO Osaka Minami Medical Center and registered at the Japan Pharmaceutical Information center (JAPIC), No. Japic CTI-070480. Written informed consent was obtained from every patient enrolled in this study. A total of 52 patients with RA (12 males and 40 females, average age 56.5 years) were enrolled in this study. All the patients were fulfilled with the 1987 ACR classification criteria for RA [3] and their radiographical stages were relatively mild less than stage II of the Steinbrocker criteria [4]. They had not been used either any disease modifying anti-rheumatic drugs (DMARDs) or corticosteroids before the entry. After the entry, they were treated according to the 2002 ACR management guideline for RA [5]. At the endpoint (24 M), more than 90 % of the patients was administered DMARDs, (methotrexate, 76.5 %, 7.8 ± 2.6 mg/week; salicylazosulfapyridine, 19.1 %; leflunomide, tacrolimus and buccilamine, <5 %), and 85.5 % of the patients received a low dose of corticosteroids (prednisolone 4.7 ± 2.8 mg/day), and 10.6 % of the patients were treated with biologics (infliximab, etanercept, tocilizumab).

Biomarkers

The candidate biomarkers were selected according to the main disease processes such as autoimmunity, inflammation and bone resorption. They were measurable in blood samples and previously suggested to be associated with bone destruction in RA [6–11]. They included rheumatoid factor-IgM (RF-IgM), RF-IgG, anti-agalactosyl IgG antibody (CARF) and anti-citrullinated peptide antibody (ACPA) for autoimmunity, C-reactive protein (CRP), erythrocyte sedimentation rate (ESR), interleukin-6 (IL6) for inflammation, type I collagen cross-linked N-telopeptide (NTx) and matrix metalloproteinase 3 (MMP3) for bone resorption, and osteopontin (Op) for inflammation and bone resorption. They were measured at the entry according to the individual standard method. Anti-CCP2 antibody was measured using the DIASTATTH Anti-CCP kit (Axis-Shiled Diagnostics Limited, United Kingdom) with the cutoff at 4.6 U/ml. IgM-RF was measured using RF-the latex X1 fixation test (DenkaSeiken, Tokyo, Japan) (cutoff value: 18 IU/ml). CARF was measured using the Eitest CA-RF enzyme immunoassay (EIA) (Sanko Junyaku, Tokyo, Japan) (cutoff value: 6.0 AU/ml). MMP-3 was measured using Panakuria MMP-3 plate for ELISA (Daiichi Fine Chemical, Toyama, Japan) (cutoff value: male 121 ng/ml, female 59.7 ng/ml). CRP was measured using high sensitivity CRP-the latex fixation test (Denka Seiken, Tokyo, Japan) (cutoff value: 0.3 mg/dl). IL-6 was measured using a sandwich ELISA kit for human IL-6 (R&D Systems Inc, Minneapolis, USA) (cutoff value: 9.96 pg/ml). OPN was measured using a sandwich ELISA kit for human OPN (Immuno-Biological Laboratories, Gunma, Japan).

Assessment of radiographical progression of bone/joint destruction (PBD)

The conventional radiographs of both hands and feet were scored on joint space narrowing (JSN) and erosions (E) according to the van der Heijde modified Sharp scores (SHS) [12] at the entry of study (A) and 24 M later (B) by two trained observers. PBD was assessed by subtracting (A) from (B), defined as ΔSHS (ΔTSS, ΔE and ΔJSN).

Statistical analyses

All statistical analyses were undertaken using the statistical package for JMP ver. 8.0 (SAS Institute, Tokyo, Japan). Associations between biomarker levels and radiographic progression (ΔSHS) were assessed by multivariate linear regression analyses with variable step-wise (backward) selection technique (cut-off $p < 0.20$). All tests were two-sided and conducted at the 0.05 significant level.

Results

Correlations between the individual biomarkers and radiographical progression (ΔSHS)

The correlations between the baseline individual biomarker and radiographical progression were presented by Pearson's correlation coefficients (Table 1).

Radiographic progressions (ΔSHS: ΔTSS, ΔE, ΔJSN) were strongly correlated with the individual baseline score (TSS*, E*, JSN*). Significant correlations ($p < 0.05$) were also noted in IL-6 and ESR for ΔTSS, in ACPA for ΔE and in IL-6 and ESR for ΔJSN. Therefore, we decided that the baseline SHS (TSS*, E*, and JSN*) was added but CARF was omitted for further statistical analyses to avoid multicollinearity because of the strong correlation ($|r| > 0.9$) with RF-IgM. ESR was also omitted because of missing data.

Table 1 Pearson 's correlation coefficients and p values

	Objective variables			Explanatory variables					
	ΔE	ΔJSN	ΔTSS	Age	E*	JSN *	TSS*	RF-IgM	RF-IgG
ΔE	1								
ΔJSN	0.4354	1							
	0.0013								
ΔTSS	0.8174	0.8743	1						
	<0.0001	<0.0001							
Age	−0.0266	−0.0099	−0.0207	1					
	0.8515	0.9447	0.8845						
E*	0.6358	0.3865	0.5900	0.0845	1				
	<0.0001	0.0047	<0.0001	0.5515					
JSN*	0.4718	0.3821	0.4988	0.2436	0.6464	1			
	0.0004	0.0052	0.0002	0.0819	<0.0001				
TSS*	0.6073	0.4234	0.5982	0.1838	0.9005	0.9139	1		
	<0.0001	0.0018	<0.0001	0.1922	<0.0001	<0.0001			
RF-IgM	0.0053	−0.0370	−0.0205	−0.0367	−0.0725	−0.0152	−0.0475	1	
	0.9712	0.8010	0.8890	0.8024	0.6204	0.9174	0.7460		
RF-IgG	0.2200	0.2474	0.2768	−0.1449	0.1515	−0.0076	0.0775	0.0244	1
	0.1373	0.0936	0.0596	0.3311	0.3092	0.9597	0.6046	0.8736	
CRP	0.0912	0.1698	0.1578	0.0773	0.0863	0.0277	0.0617	−0.0371	0.1415
	0.5201	0.2287	0.2638	0.5861	0.5428	0.8456	0.6638	0.8004	0.3428
ESR	0.2833	0.5492	0.4801	0.1756	0.1611	0.1023	0.1407	−0.1506	0.2175
	0.1441	0.0025	0.0097	0.3713	0.4128	0.6046	0.4751	0.4534	0.2858
MMP3	0.2003	−0.0207	0.0955	0.2420	0.4288	0.1315	0.3049	−0.0688	0.0112
	0.1771	0.8902	0.5231	0.1013	0.0026	0.3781	0.0372	0.6534	0.9406
NTx	−0.0963	−0.0269	−0.0694	0.2730	−0.0109	−0.0964	−0.0598	−0.1142	0.0089
	0.5197	0.8574	0.6431	0.0634	0.9420	0.5194	0.6898	0.4551	0.9529
IL-6	0.2078	0.4461	0.3969	0.0920	0.1697	0.1985	0.2037	−0.0915	0.2672
	0.1520	0.0013	0.0047	0.5294	0.2438	0.1715	0.1603	0.5407	0.0760
CCP	0.3252	0.0405	0.2059	−0.1457	0.0506	0.1378	0.1039	0.0854	0.3844
	0.0334	0.7966	0.1854	0.3511	0.7473	0.3781	0.5075	0.5909	0.0109
CARF	−0.0482	−0.0159	−0.0363	0.0863	−0.0578	0.1561	0.0562	0.9378	−0.0829
	0.7476	0.9155	0.8087	0.5635	0.6995	0.2946	0.7077	<0.0001	0.5795
OPN	−0.0297	0.1298	0.0671	−0.1721	−0.122	−0.1172	−0.1371	0.1309	0.1421
	0.8345	0.3590	0.6367	0.2224	0.3887	0.4080	0.3519	0.3702	0.3408

Table 1 continued

	Explanatory variables							
	CRP	ESR	MMP3	NTx	IL-6	CCP	CARF	OPN
ΔE								
ΔJSN								
ΔTSS								
Age								
E*								
JSN*								
TSS*								
RF-IgM								
RF-IgG								
CRP	1							
ESR	0.6462	1						
	0.0002							
MMP3	0.0678	0.2626	1					
	0.6505	0.1949						
NTx	0.0604	0.3458	0.1213	1				
	0.6866	0.0836	0.4166					
IL-6	0.1688	0.5170	0.1524	0.3622	1			
	0.2464	0.0081	0.3177	0.0145				
CCP	−0.1274	0.1804	−0.0986	−0.2524	−0.1390	1		
	0.4155	0.4102	0.5295	0.1025	0.3800			
CARF	−0.1090	−0.1523	−0.0427	−0.1382	−0.1694	0.1963	1	
	0.4659	0.4576	0.7755	0.3541	0.2658	0.2071		
OPN	0.2664	0.2633	−0.1070	0.1158	0.2981	−0.0968	−0.1686	1
	0.0563	0.1759	0.4743	0.4381	0.0375	0.5367	0.2572	

The correlations between the individual biomarker and radiographical progression were presented by Pearson's correlation coefficients. Radiographic progression (ΔSHS: ΔTSS, ΔE, ΔJSN) were strongly correlated with the individual baseline score (TSS*, E*, JSN*). In addition, significant correlations ($p < 0.05$) were noted in IL-6 and ESR for ΔTSS, in ACPA for ΔE and in IL-6 and ESR for ΔJSN. The correlation between RF-IgM and CARF was strong ($|r| > 0.9$)

Upper line: correlation coefficients; lower line: p values

Assessment of associations between the baseline biomarkers and ΔSHS by multivariate regression analyses with step-wise selection

At the first step, multivariate regression analyses were performed in all variables except ESR and CARF. Then, the variables were deleted one by one (cutoff $p < 0.2$) and the analyses were repeated. Finally, for ΔTSS, IL-6 and ACPA as well as TSS* were selected. For ΔE, ACPA and E*were selected. For ΔJSN, IL-6 and JSN* score were selected. Then, the final analysis was performed using these selected variables. As a result shown in Table 2, the associations remained significant in IL-6 ($p = 0.0091$) as well as in TSS* ($p = 0.0001$) but not in ACPA ($p = 0.1176$) for ΔTSS. For ΔE, ACPA showed significant associations ($p = 0.0129$) as well as E* ($p < 0.0001$). For ΔJSN, IL-6 still showed significant associations ($p = 0.0039$) as well as JSN* ($p = 0.0262$).

Discussion

The aim of this prospective study was to seek for a useful and convenient biomarker to predict PBD in mild radiographic stages of RA under the real clinical circumstances. The candidate biomarkers in this study were selected by taking consideration into the main pathogenic disease processes such as autoimmunity, inflammation and bone resorption. There were two main findings. Firstly, the baseline SHS (TSS*, E*, JSN*) significantly correlated with PBD (ΔTSS, ΔE and ΔJSN). All patients enrolled in this study had short disease duration (<2 years) and with mild bone destruction (less than stage II of the Steinbrocker classification). They still stayed at so-called "the Window of Opportunity" stage. This strongly suggests and supports the importance of earlier therapeutic interventions in RA as emphasized in lots of previous clinical studies [1].

Secondly, among the candidate biomarkers, the baseline serum ACPA titers and IL-6 levels showed significant associations with PBD. It is not surprising that ACPA is a significant predictor for PBD and their titer is important [7, 13]. We also previously reported that the usefulness of prediction for on-set of RA in undifferentiated polyarthritis [14]. These seem to be reasonable because ACPA is categorized into a biomarker for autoimmunity which is an earlier event in the pathogenesis of RA compared to the other subsequent events such as inflammation and tissue damages (bone/cartilage resorption). Another reason is that ACPA is more specific for autoimmunity in RA than other biomarkers such as RF-Igs (RF-IgM and RF-IgG) [8, 14]. On the other hand, there have been lots of supportive reports which suggest that MMP-3 is useful for predicting PBD in RA [10], they were not significantly associated with ΔSHS in this prospective study. The reason for this discrepancy is not clear. However, this suggests that MMP-3 might reflect on ongoing inflammation and bone/cartilage destruction in the affected joints rather than the trigger [15] because proinflammatory cytokines induce MMPs, including MMP-3 [16].

In this study, we also showed IL-6 was a significant predictor for PBD in early stages of RA. IL-6 is well known as one of the major proinflammatory cytokines in the pathogenesis of RA as well as TNF and IL-1 [17]. In addition, it has been revealed as an important therapeutic target [17]. In fact, recent clinical trials have shown an outstanding efficacy of anti-IL-6 therapy in RA [18]. Besides IL-6, other proinflammatory cytokines, such as TNFα and IL-1, especially TNFα is interesting as a candidate marker as well as IL-6, because it is well known that TNFα is one of the key cytokines in the pathogenesis of RA, and TNF inhibitors are major biologics in the treatment of RA. We tried to measure serum TNFα levels in the RA patients by using a sandwich ELISA kit (QTA00B) for human TNFα (R&D System Inc, Minneapolis, USA), however, all of the serum TNFα levels of the patients were within the range of the healthy volunteers (not detectable ~9.03 pg/ml). So, TNFα was not included as a candidate marker in this study.

Table 2 Multivariate analysis with selected variables

Variable	Regression coefficient	p value
(A) ΔTSS		
TSS*	0.1819	0.0001
IL-6	0.1358	0.0091
ACPA	0.0051	0.1176
(B) ΔE		
E*	0.2298	<0.0001
ACPA	0.0044	0.0129
(C) ΔJSN		
JSN*	0.1165	0.0262
IL-6	0.1010	0.0039

Associations between biomarkers levels and radiographic progression (ΔSHS) were assessed by multivariate linear regression analyses with variable step-wise (backward) selection technique. At the first step, multivariate regression analyses were undertaken in all variables except ESR and CARF. Then, the variables were deleted one by one (cutoff $p < 0.2$) and the analyses were repeated. Finally, in ΔTSS, IL-6 and ACPA as well as the baseline TSS (TSS*) were selected. In ΔE, ACPA and the baseline E score (E*) were selected. In ΔJSN, IL-6 and the baseline JSN score (JSN*) were selected. Then, the final analysis was performed using these selected variables. The associations remained significant for IL-6 ($p = 0.0091$) as well as the baseline TSS ($p = 0.0001$) but not for ACPA ($p = 0.1176$) in ΔTSS. In ΔE, ACPA showed significant associations ($p = 0.0129$) as well as the baseline E score ($p < 0.0001$). In ΔJSN, IL-6 still showed significant associations ($p = 0.0039$) as well as the baseline JSN score ($p = 0.0262$). All tests were two-sided and conducted at the 0.05 significant level

On the other hand, as mentioned above, anti-cytokine therapies especially using biologics is now well known like a master of treatment of RA. However, they have some critical concerns such as severe adverse effects and high costs. In addition, we are not able to know which cytokine is the most optimal target before the start of the treatment. The finding suggests that the early stages of RA patients showing high serum IL-6 levels might be good candidates for anti-IL6 therapy. Another advantage of IL-6 is that it reflects on the actual degree of inflammation and it can be measured easily and accurately in sera. It also changes more dynamically in sera compared to TNF and IL-1 [19].

In summary, both the baseline ACPA titers and serum IL-6 levels as well as the baseline SHS (TSS*, E*, JSN*) correlated with PBD, suggesting that ACPA and serum IL-6 levels have potentials for predicting PBD in early stages of RA and earlier therapeutic intervention is also important.

Acknowledgments This work was supported by a Grant-in-Aid for Research of Immunological Disorders from The Japan National Hospital Organization (NHO) and carried out by the iR-net Study Group of NHO. We thank Drs. Yasuda M. and Fujita M. for recruiting the patients and Mr. Yano T. for helping statistical analyses. We also thank Ms. Kitatobe, Ms. Nakata and Ms. Uesugi for their excellent secretarial works.

Conflict of interest All authors have no conflicts of interest.

References

1. Quinn MA, Conaghan PG, Emery P (2001) The therapeutic approach of early intervention for rheumatoid arthritis: what is the evidence? Rheumatology (Oxford) 40:1211–1220
2. Smolen JS, Aletaha D, Grisar J et al (2008) The need for prognosticators in rheumatoid arthritis. Biological and clinical mar: where are we now? Arthritis Res Ther 10:208
3. Arnett FC, Edworthy SM, Bloch DA, McShane DJ, Fries JF, Cooper NS et al (1988) The American Rheumatism Association 1987 revised criteria for the classification of rheumatoid arthritis. Arthritis Rheum 31:315–324
4. Steibrocker O, Traeger CH, Batterman RC (1949) Therapeutic criteria in rheumatoid arthritis. J Am Med Assoc 140:659–662
5. Amenrican College of Rheumatology Sucommittee on Rheumatoid Arthritis Guidelines (2002) Guidelines for the management of rheumatoid arthritis. 2002 Update 46:328–346
6. Dawes PT, Fowler PD, Clarke S, Fisher J, Lawton A, Shadforth MF (1986) Rheumatoid arthritis: treatment which controls the C-reactive protein and erythrocyte sedimentation rate reduces radiographic progression. Br J Rheumatol 25:44–49
7. van Venrooij WJ, Hazes JM, Visser H (2002) Anticitrullinated protein/peptide antibody and its role in the diagnosis and prognosis of early rheumatoid arthritis. Neth J Med 60:383–388
8. Young A, Sumar N, Bodman K, Goyal S, Sinclair H, Roitt I, Isenberg D (1991) Agalactosyl IgG: an aid to differential diagnosis in early synovitis. Arthritis Rheum 34:1425–1429
9. Green MJ, Gough AK, Devlin J, Smith J, Astin P, Taylor D et al (2003) Serum MMP-3 and MMP-1 and progression of joint damage in early rheumatoid arthritis. Rheumatology 42:83–88
10. Valleassion H, Laasonen L, Koivula MK, Mandelin J, Friman C, Risteli J et al (2003) Two year randomized controlled trial of etidronate in rheumatoid arthritis: changes in serum amino terminal telopeptides correlate with radiographic progression of disease. J Rheumatol 30:468–473
11. Ohshima S, Yamaguchi N, Nishioka K, Mima T, Ishii T, Umeshita-Sasai M et al (2002) Enhanced local production of osteopontin in rheumatoid arthritis. J Rheumatol 29:979–990
12. Van der Heijde DM, van Riel PL, Nuver-Zwart IH, Gribnau FW, van de Putte LB (1989) Effects of hydroxychloroquine and sulphasalazine on progression of joint damage in rheumatoid arthritis. Lancet 1:1036–1038
13. Syversen SW, Gaarder PI, Goll GL, Odegard S, Haavardsholm EA, Mowinckel P et al (2008) High anti-cyclic citrullinated peptide levels and an algorithm of four variable predict radiographic progression in patients with rheumatoid arthritis: results from a 10-year longitudinal study. Ann Rheum Dis 67:212–217
14. Kudo-Tanaka E, Ohshima S, Ishii M, Mima T, Matsushita M, Azuma N et al (2007) Autoantibodies to cyclic citrullinated peptide 2 (CCP2) are superior to other potential diagnostic biomarkers for predicting rheumatoid arthritis in early undifferentiated arthritis. Clin Rheumatol 26:1627–1633
15. Syversen SW, Haavardsholm EA, Boyesen P, Goll GL, Okkenhaug C, Gaarder PI et al (2010) Biomarkers in early rheumatoid arthritis: longitudinal associations with inflammation and joint destruction measured by magnetic resonance imaging and conventuinal radiographs. Ann Rheum Dis 69:845–850
16. Suzuki M, Hashizume M, Yoshida H, Shiina M, Mihara M (2010) IL-6 and IL-1 synergistically enhanced the production of MMPs from synovial cells by up-regulating IL-6 production and IL-1 receptor I expression. Cytokine 51:178–183
17. Nishimto N, Kishimoto T (2006) Interleukin-6: from bench to bedside. Nat Clin Pract Rheumatol 2:619–626
18. Smolen JS, Beaulieu A, Rubbert-Roth A, Ramos-Remus C, Rovensky J, Alecock E et al (2008) Effect of interleukin-6 receptor inhibition with tocilizumab in patients with rheumatoid arthritis (OPTION study): a double-blind, placebo controlled, randomized trial. Lancet 371:987–997
19. Ohshima S, Saeki Y, Mima T, Sasai M, Nishioka K, Shimizu M et al (1999) Long-term follow-up of the changes in circulating cytokines, soluble cytokine receptors, and white blood cells subset counts in patients with rheumatoid arthritis (RA) after monoclonal anti-TNF alpha antibody therapy. J Clin Immunol 19:305–313

二光子励起顕微鏡による生きた組織の観察

Visualization of live tissues and organs by using intravital two-photon microscopy

石井　優

Key Words: live imaging, two-photon microscopy, immune system, bone homeostasis, chemokine

Abstract

動物の本質は＜動き＞にあるが，これは生体のみが備え，死体にはない。近年，蛍光顕微鏡技術の長足の進歩により，生体を「生きたまま」で観察することができるようになった。この技術によって，特にそれまで見えなかった細胞や分子の「動き」を直接見ることができるようになり，生命科学の領域にパラダイムシフトがもたらされつつある。本稿では，二光子励起顕微鏡を用いた「生体イメージング」の方法論と今後の応用について概説する。

■二光子励起顕微鏡の原理と応用

蛍光観察では，注目する細胞や分子などを蛍光分子で標識する。蛍光分子は一般に，エネルギー的に低い状態（基底状態）と高い状態（励起状態）があるが，普段は基底状態にある。このエネルギー差に相当する光（光子）を当てると，蛍光分子はこのエネルギーを吸収して励起状態になるが，自然にまた励起状態へと戻っていく（図上）。この際，そのエネルギーに相当する光を放出し，これを観察しているのが蛍光観察である。

二光子励起とは，蛍光観察の際に，光子１個ではなく，２個の光子を蛍光分子に同時に当てることにより励起させることである。光子１個　対　蛍光分子１個　による１対１反応に比べて，複数の光子による励起（多（二）光子励起）は極めて起こりにくい現象であるが，光子密度を非常に高くすれば非線形的に起こり得る（Göppert-Mayer, 1931）。

Masaru Ishii, M.D., Ph.D.
大阪大学免疫学フロンティア研究センター・細胞動態学分野
Professor and Chief, Laboratory of Cellular Dynamics, Immunology Frontier Research Center (IFReC), Osaka University

この「二光子励起」の現象は，光子密度が異常に高い場所でのみ起こる。蛍光顕微鏡でいえば，光が一点に凝集される点，すなわち「焦点」のみで起こり得る現象である。これを利用して「焦点のみで励起が起こるような顕微鏡」として「二光子励起顕微鏡」が作られた[1]。

まとめると，この顕微鏡には以下のような長所がある。

① 高い空間（z軸）解像度

焦点平面のみでしか励起が起こらない（その他の平面では励起に必要なエネルギーに満たない光子が当たっているものの励起には至らない）ため，非観察面からの蛍光シグナルがない（非観察面からの蛍光シグナルは「ピンボケ」の原因となる）。

② 高い組織透過性（深部組織の観察に威力を発揮）

２個の光子を同時に当てて蛍光分子を励起するため，当てる光子１個分のエネルギーは小さくて済む（約半分）。エネルギーが半分ということは，光子の波長が２倍になることであり，実際二光子励起で用いるレーザーは近赤外域にある（波長が780～1000 nm）。波長が長い赤外光は，短い可視光や紫外光よりも浸透性が高く，深い組織まで励起・観察することが可能となる。

これらの特長は，「組織・臓器を生かしたままで観察」するために極めて有用である。固定した（もはや生きていない）組織や臓器は，パラフィンなどで包埋して薄切すれば，どんな場所でも観察できるが，生きた組織（特に生きた個体内）では，観察したい場所が対物レンズでアプローチできる場所よりも深いことがある。このような場合，二光子励起顕微鏡が威力を発揮する。

■生きた組織・個体の観察の実際

「生体イメージング」は大きく2つに分類される。「tissue explant imaging」では，実験動物を屠殺して注目する組織・臓器を取り出し，酸素化した培養液中で生かして観察する。一方，「intravital imaging」では，動物を麻酔下で生かしたままで，観察したい組織・臓器を露出して観察する。Intravitalの方法論はより困難であるが多くの利点があり，特に，動物を生かしているので循環血流が保たれる点は非常に大きい。これは，特に免疫・血液系のように，血流を介した細胞の動態が重要なシステムの解析に有用である[1-3]。

■生きた骨組織・骨髄内の二光子励起観察

筆者はintravital two-photon imagingによる，生きた骨組織・骨髄内の高解像度イメージング法を世界に先駆けて開発した。硬い石灰質に囲まれた骨組織の内部は，生きたままでの観察が特に困難であると考えられていた。骨基質に含まれるリン酸カルシウム結晶は，励起光を容易に散乱させるため，二光子励起に用いる近赤外線レーザーを用いても深部まで到達させることは難しかった。筆者はシステムを改良し，骨基質が比較的薄いマウス頭頂骨を用いて，生きた骨髄内を外部から非侵襲的に高解像度で観察できる実験系を確立した（図下）[4,5]。これを用いて，骨髄内の細胞が血中から遊走したり逆に再還流する様子をリアルタイムで可視化し，この動態を制御するケモカインを同定した[4]。

骨髄には雑多な血液系・間葉系細胞が，所狭しと詰め込まれている。多様な血液系細胞はそれぞれ決まった場所（ニッチ）に存在し，また互いに複雑な静的・動的ネットワークを形成しているが，これらについては未だ不明な点が数多く残されており，二光子励起顕微鏡による“非破壊検査”を用いた今後の解明が期待される。

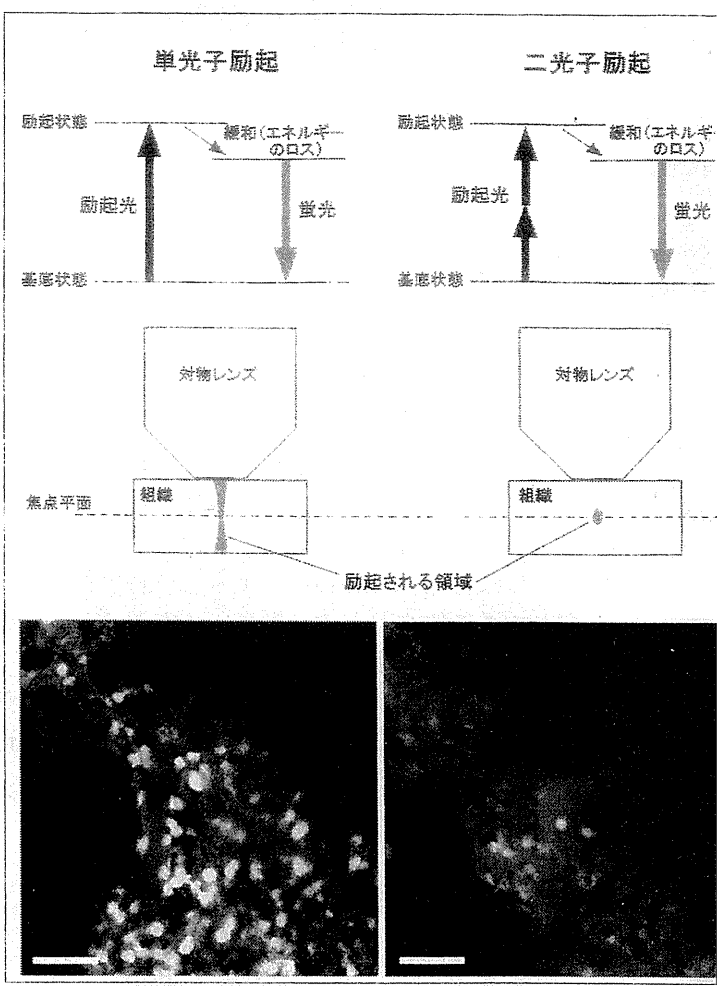

図　二光子励起顕微鏡の原理とその生体観察
上図：通常の蛍光観察では，1個の蛍光分子を1個の光子で励起するが（左図），多（二）光子励起では複数（2個）の光子で励起する（右図）。このような現象は非常に起こりにくく，光子密度が極大となる焦点平面のみで起こる（下図）。このため，観察したい部位のみ蛍光することになるので高い空間解像度が得られ，非観察部位が励起されないため光毒性が低く退色が少ない。
下図：顆粒球系（LysM$^+$；左側）および単球系（CX$_3$CR1$^+$；右側）をそれぞれGFP標識したトランスジェニックマウスの骨髄腔の生体二光子励起イメージング。骨髄内の血管構造をTexas Redを結合した高分子デキストランを静脈注射にて可視化している。実際にはこれを一定時間間隔で撮影し，動画を作成する（文献[4]より一部改変；動画については筆者HP<http://bioimaging.ifrec.osaka-u.ac.jp>を参照）。スケールバー：30 μm。

文　献
1) Denk W, Strickler JH, Webb WW. Science. 248: 73-76, 1990.
2) Stoll S, Delon J, Brotz TM, Germain RN. Science. 296: 1873-1876, 2002.
3) Miller MJ, Wei SH, Parker I, Cahalan MD. Science. 296: 1869-1873, 2002.
4) Ishii M, Egen JG, Klauschen F, Meier-Schellersheim M, Saeki Y, Vacher J, Proia RL, Germain RN. Nature. 458: 524-528, 2009.
5) Klauschen F, Ishii M, Qi H, Bajénoff M, Egen JG, Germain RN, Meier-Schellersheim M. Nature Protoc. 4: 1305-1311, 2009.

破骨細胞のイメージングとRANKLシグナル

菊田 順一[*1] 石井 優[*2]

破骨細胞は，単球系血液細胞から分化・成熟する多核巨細胞であり，「骨吸収」という特殊な機能を持つ唯一の細胞である。しかし，生きた骨組織内で成熟破骨細胞がどのように骨吸収を行っているのか，生体内における成熟破骨細胞の動態についてはこれまで明らかにされてこなかった。我々は最近，二光子励起顕微鏡を駆使することでマウスを生かしたまま，骨表面上での生きた成熟破骨細胞の動態を可視化することに成功し，成熟破骨細胞の骨吸収がRANKL（receptor activator of NF-κB ligand）によって動的に制御されていることを明らかにした。

本稿ではこの研究成果に加え，我々が開発した骨のライブイメージングの方法論やその応用について概説する。

RANKL signaling and bone diseases.

In vivo imaging of mature osteoclasts and RANKL signaling.

Laboratory of Cellular Dynamics, Immunology Frontier Research Center, Osaka University.

Junichi Kikuta, Masaru Ishii

Osteoclasts are 'bone-resorbing' giant polykaryons that differentiate from mononuclear macrophage/monocyte-lineage hematopoietic precursors. However how the activity of mature osteoclasts is regulated *in vivo* remains unclear. To answer the question, we utilized an advanced imaging system for visualizing live bone tissues with intravital multiphoton microscopy that we have recently established. By means of the system we have recently succeeded in visualization of mature osteoclasts in live bones and revealed that RANKL regulates bone-resorptive functions of mature osteoclasts *in vivo*. Here we show the latest data and the detailed methodology of intravital imaging of bone tissues, and also discuss its further application.

はじめに

破骨細胞は単球系血液細胞から分化・成熟する多核巨細胞であり，「骨吸収」という特殊な機能を持つ唯一の細胞である。骨髄から採取した単球系細胞をM-CSF（macrophage colony-stimulating factor）とRANKL（receptor activator of

大阪大学 免疫学フロンティア研究センター 細胞動態学 [*1]（きくた・じゅんいち） [*2]教授（いしい・まさる）

NF-κB ligand)の刺激下で*in vitro*で培養すると，破骨細胞様の多核巨細胞が形成され，中には100核以上の巨細胞も観察される。しかし「このような多核巨細胞が*in vivo*でも本当に形成されるのか」，「生きた骨組織内で成熟破骨細胞はどのように骨吸収を行うのか」など，生体内での成熟破骨細胞の動態についてはこれまで明らかにされてこなかった。

硬い石灰質に囲まれた骨組織の内部は従来生きたままでの観察が困難であったが，我々は，組織深部の観察が可能な「二光子励起顕微鏡」を駆使して，マウスを生かしたままで骨組織内の細胞動態を観察するイメージング方法を確立した[1]。この方法を用いて，我々は最近，骨表面上での生きた成熟破骨細胞の動態を可視化することに成功し，成熟破骨細胞の骨吸収がRANKLによって動的に制御されていることを明らかにした。

本稿では，これらの研究成果の解説に加えて骨組織内の生体二光子励起イメージングの方法論や，その今後の応用と将来性について，実際の画像を紹介しながら概説する。

骨組織内の生体二光子励起イメージング

1．二光子励起顕微鏡のメリット

二光子励起顕微鏡では，通常の蛍光顕微鏡観察(共焦点レーザー顕微鏡も含む)で用いる励起光の半分のエネルギー(2倍の波長)をもったレーザー光を，細かいパルス状に放出したものを励起光源に用いる。二光子励起は，レンズで集約された光子が集まる1点の焦点面にしか起こらないため，非常にクリアな画像が得られ(高い空間解像度)，観察対象となる組織・臓器への光毒性や蛍光の退色もきわめて小さく抑えることができる(低い組織侵襲性)。また，励起光として通常の半分のエネルギー(2倍の波長)の近赤外光(波長が780～1,000 nm)を用いるため，組織の深部まで励起光を到達させることができる(高い組織透過性)。以上の特長から，二光子励起顕微鏡は，「組織・臓器を生かしたままで観察」するためにきわめて有用である[2,3]。

2．骨組織内の“生体(＝intravital)”イメージングの実際

骨基質に含まれるリン酸カルシウム結晶は，励起光を容易に散乱させるため，二光子励起に用いる近赤外線レーザーを用いても深部まで到達させることは難しい。現在の近赤外線レーザーでは，軟部組織であれば表面から800～1,000 μmまで到達が可能であるが，骨組織の場合は，150～200 μmが限界である。このため，我々は，骨基質が薄くて骨表面から骨髄腔まで80～120 μmで到達できるマウスの頭頂骨を用いて，骨組織内の生体イメージングに取り組んでいる[1,4-6]（図1）。実際には，麻酔したマウスの頭頂骨の皮膚を切開し，露出させた後，顕微鏡用のステージにマウスを固定して観察する。この方法では，骨髄腔内を流れる蛍光色素を血流が供給されているため，骨組織に定着している細胞の動きのみならず，血管から骨髄内へ細胞が流入したり，逆に血中へ還流していく様子を観察することができる。さらには，薬剤を尾静脈などから全身投与すると，血流を通して速やかに観察部位に到達させることができる。

この「生体二光子励起イメージング」を用いて，我々はこれまで，破骨前駆細胞の骨吸収面への遊走・接着が，脂質メディエーターの一種であるスフィンゴシン1リン酸(S1P)によって動的に制御されていることを解明した[1,5]。しかしながら，

RANKL：receptor activator of nuclear factor-κB ligand（破骨細胞分化因子）
M-CSF：macrophage colony-stimulating factor（マクロファージコロニー刺激因子）
S1P：sphingosine-1-phosphate（スフィンゴシン1リン酸）

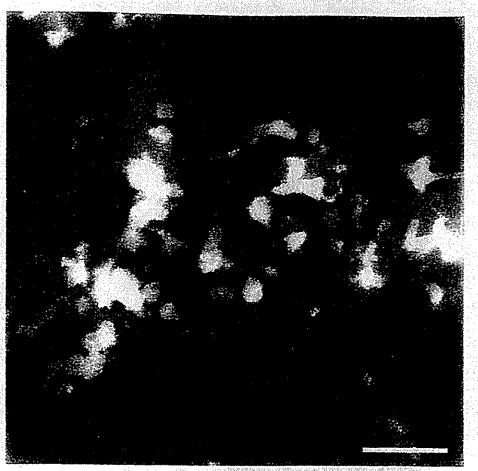

図1　骨組織内での破骨前駆細胞の生体二光子励起イメージング

破骨前駆細胞を含む単球系細胞を緑色にラベルしたマウスの骨髄腔の生体二光子励起イメージング。骨髄腔内の血管構造は，赤色蛍光（Texas Red）を結合させた高分子デキストランを静脈注射して可視化している。青色は骨組織を示す。実際の実験ではこれを一定時間間隔で撮影し，動画を作成する。
（スケールバー：30 μm）
（カラーグラフ，ページ5頁参照）（筆者作成）

「破骨前駆細胞が骨表面に到達して成熟破骨細胞に分化した後，骨吸収が生体内でどのように調節されているのか」という点については，これまで明らかにされてこなかった。そこで，我々はさらに，「生体二光子励起イメージング」技術を駆使して，生体骨組織内での成熟破骨細胞の動態を可視化することに取り組んだ。

生体イメージングによる成熟破骨細胞の動態解明

1．生きた成熟破骨細胞の動態の可視化

我々は，成熟破骨細胞に特異的に緑色蛍光蛋白質（GFP）を発現させたマウスの骨組織内を二光子励起顕微鏡で観察することにより，生きた成熟破骨細胞の動態の可視化に成功した（図2a）。その結果，骨表面で骨吸収を行っている成熟破骨細胞には，「①動きがなく，今まさに骨吸収をしている状態の細胞（図2b）」と，「②動いていて，骨吸収をしていない状態の細胞（図2c）」の少なくとも2種類が存在することが明らかとなった（論文投稿中）。

次に我々は，これらのマウスに各種薬剤を投与して，成熟破骨細胞の動態の変化を検討した。まず，成熟破骨細胞を蛍光標識したマウスにRANKLを腹腔内投与して破骨細胞の機能を亢進させ，投与2日後にマウスの骨組織内を生体二光子励起顕微鏡で観察した。その結果，成熟破骨細胞数が増加し，そのほとんどが「①動きがなく，今まさに骨吸収をしている状態の細胞」であった。一方，骨粗鬆症の治療薬であるビスホスホネートを投与して破骨細胞の機能を抑制させると，骨表面での成熟破骨細胞数が減少し，また残った細胞のほとんどが，「②動いていて，骨吸収をしていない状態の細胞」であった。このように，二光子励起イメージングを用いることにより，成熟破骨細胞の絶対数のみならず，成熟破骨細胞の機能（骨吸収をしているのか，あるいは骨吸収をしていないのか）も同時に評価することができるようになった。

2．RANKLによる成熟破骨細胞の骨吸収制御機構の解明

次に我々は，上述の成熟破骨細胞を蛍光標識したマウスにRANKLを急速に静脈内投与した。その結果，投与後30分という比較的短い時間に，成熟破骨細胞が「②骨吸収をしていない状態」から「①今まさに骨吸収をしている状態」へと変わっていく様子が観察された。従来，RANKLは破骨前駆細胞が成熟破骨細胞へ分化するための必須の因子であることが知られていた。今回我々が行ったイメージングの結果により，RANKLは破

GFP：green fluorescence protein, green fluorescent protein ともいう。（緑色蛍光タンパク質）

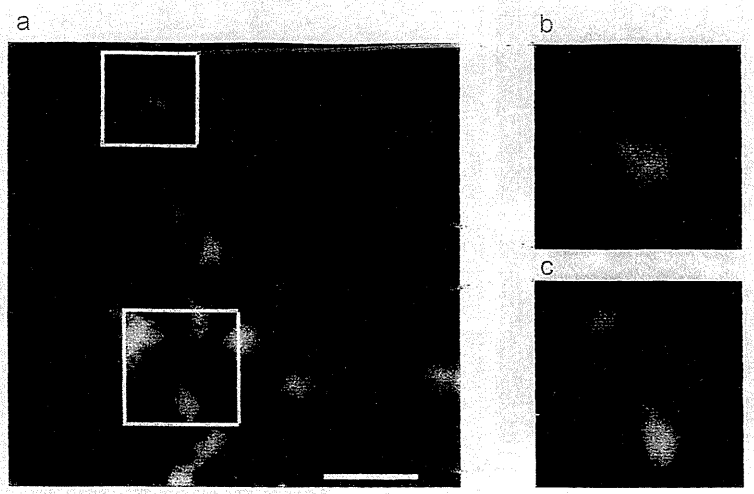

図2　骨組織内での成熟破骨細胞の生体二光子励起イメージング

成熟破骨細胞を緑色にラベルしたマウスの骨髄腔の生体二光子励起イメージング（a）。骨髄腔内の血管構造は，赤色蛍光（Texas Red）を結合させた高分子デキストランを静脈注射して可視化している。青色は骨組織を示す。骨表面で骨吸収を行っている成熟破骨細胞には，「動きがなく，今まさに骨吸収をしている状態の細胞（b）」と，「動いていて，骨吸収をしていない状態の細胞（c）」の少なくとも2種類が存在する。
（スケールバー：40μm）　（カラーグラフィック5頁参照）（筆者作成）

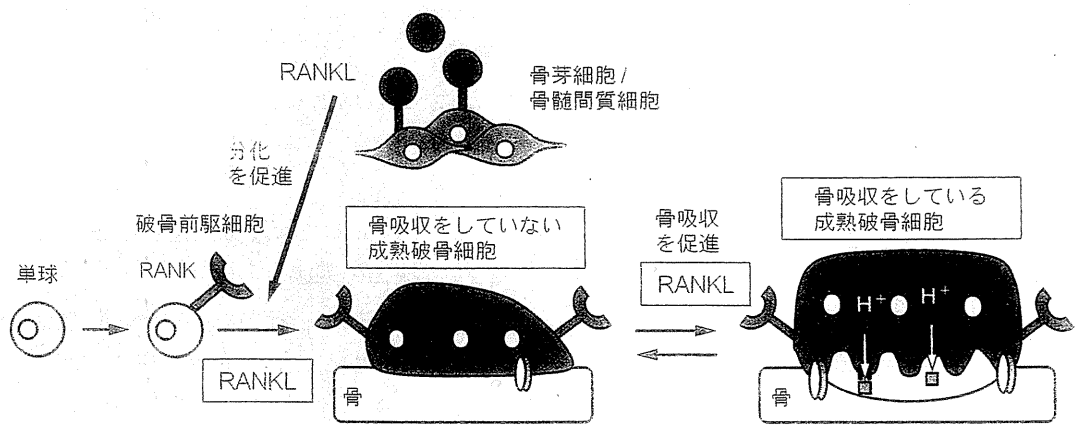

図3　生体内における成熟破骨細胞の骨吸収メカニズム

成熟破骨細胞には，「骨吸収をしていない状態の細胞」と，「今まさに骨吸収している状態の細胞」との2種類が存在する。また，RANKLは破骨細胞分化を促進するだけでなく，成熟した破骨細胞にも作用し，骨吸収を促進する役割も担っている。（筆者作成）

骨細胞の分化を促進するだけでなく，成熟した破骨細胞にも作用し，骨吸収を促進する役割も担っていることが明らかとなった（図3）。

これまでの成熟破骨細胞の骨吸収に関する研究のほとんどは，固定した骨組織を切り出して行われたものであるため，細胞の動的な情報を得るこ

とが困難であった。しかし，今回我々が行ったイメージング系は，マウスを生かしたまま，骨表面での成熟破骨細胞の骨吸収の動態をリアルタイムで観察することができるため，今後，骨吸収性疾患の病態解明や新規薬剤の開発においても強力な手段となり得ると考えられる。

今後の展開

1．頭頂骨以外の骨組織のイメージング系の開発

現時点では，十分な解像度で可視化できる骨組織は，骨梁が薄くレーザー光を透過させやすい頭頂骨に限られている。基本的には，どこの部分の骨であっても，骨代謝や骨髄細胞の動態などには変化がないと考えられるが，それらを実証するためには，やはり長管骨など一般に広く研究に用いられている骨組織をライブイメージングにより解析する必要がある。現在我々は，長管骨のライブイメージング系の確立に取り組んでいる。

2．長時間のライブイメージング系の開発

ガス麻酔下でマウスを生かしたままで，骨組織を手術的に露出してイメージングに当たっている現在の方法では，連続した撮影時間は4～5時間程度が限界である。細胞の動きや細胞間の接触時間などをイメージングするのであれば，この観察時間で十分であるが，それより長い時間のかかる現象(例えば，破骨細胞の分化など)をイメージングするためには，別の測定系を構築する必要がある。(マウスを長期間にわたり麻酔管理するか，手術野を閉じて経日的観察を可能にするなど)。現在我々は，長時間のライブイメージング系の確立にも取り組んでいる。

おわりに

近年の蛍光イメージング技術の急速な進歩のおかげで，さまざまな臓器・組織での生きた細胞の観察が活発に行われている。しかしながら，これまでの生体イメージング研究の多くは，生体内での細胞の動き(動く速さ)や細胞間相互作用(細胞同士の接触時間)を観察するにすぎなかった。これからの生体イメージング研究では，「細胞が動いて接触した後に何が起こるのか」，すなわち生体内での細胞の「機能」や「分化」をイメージングすることが重要になってくると思われる。特に骨組織は，破骨細胞や骨芽細胞による骨代謝制御の場であるばかりでなく，リンパ球を始めとして顆粒球・単球など多種多様な血液細胞の発生・機能分化にとって重要な部位である。我々が開発した骨組織の生体二光子励起イメージングの方法論は，骨髄腔内での各細胞の挙動・位置決めとその分化制御や，血液系幹細胞が多能性を維持する特殊な環境(ニッチ)の解明において強力な手段となることが強く期待される。

文　献

1) Ishii M, Egen JG, Klauschen F, et al : Sphingosine-1-phosphate mobilizes osteoclast precursors and regulates bone homeostasis. Nature 458 (7237) : 524-528, 2009.
2) Denk W, Strickler JH, Webb WW : Two-photon laser scanning fluorescence microscopy. Science 248 (4951) : 73-76, 1990.
3) Denk W, Svoboda K : Photon upmanship : why multiphoton imaging is more than a gimmick. Neuron 18 (3) : 351-357, 1997.
4) 島津　裕，石井　優：生体2光子励起顕微鏡による骨組織ライブイメージング．実験医学 28 (13) : 2147-2153, 2010.
5) Klauschen F, Ishii M, Qi H, et al : Quantifying cellular interaction dynamics in 3-D fluorescence microscopy data. Nat Protoc 4 (9) : 1305-1312, 2009.
6) Ishii M, Kikuta J, Shimazu Y, et al : Chemorepulsion by blood S1P regulates osteoclast precursor mobilization and bone remodeling in vivo. J Exp Med 207 (13) : 2793-2798, 2010.